Indian Journal of Engineering & Materials Sciences
Vol. 31, August 2024, pp. 515-523
DOI: 10.56042/ijems.v31i4.10038

Optimization of process parameters of laser composite surfaced Ti-13Nb-13Zr using Taguchi method

Tapas Bera[a], Indranil Manna[a, b], Esther Titilayo Akinlabi[c] & Jyotsna Dutta Majumdar[d*]

[a]Department of Metallurgical & Materials Engineering, Indian Institute of Technology Kharagpur, West Bengal, 721302, India

[b]Birla Institute of Technology, Ranchi, Jharkhand, 835215, India

[c]Northumbria University, Ellison Pl, Newcastle upon Tyne NE1 8ST, UK

Received: 31 March 2024; Accepted: 18 May 2024

In the current study, laser composite surfacing (LCS) of Ti-13Nb-13Zr alloy has been undertaken by preplacing graphite coating (thickness of 250 µm) and subsequent laser melting with a 6 kW fibre optics delivered diode laser (mode: continuous wave) at varied power and scan speed. Based on the performance of the surface measured by microhardness, wear, and corrosion resistance; process parameters are optimized utilizing the Taguchi method. Analysis is conducted by the grey relational grade (GRG) and signal-to-noise (S/N) ratios of the output parameters. The derived optimal parameters are 1000 W applied power and 20 mm/s scan speed. Maximum improvement in microhardness (by 2 times), nanohardness (by 2.6 times), wear resistance (by 5.8 times) and corrosion resistance properties (by 6 times) are achieved after the LCS process. The investigation helps to establish an efficient process for Ti-13Nb-13Zr alloy fabricated by LCS.

Keywords: Ti-13Nb-13Zr, Laser Composite Surfacing, Optimization, Taguchi Method, S/N ratio

1 Introduction

Ti-13Nb-13Zr is an important category of titanium-based alloy having a density of 4.99 kg/m^3, Young's modulus of 79 GPa and tensile strength varying from 705-1035 MPa[1]. Due to its higher specific strength and lower Youngs modulus, this alloy has gained popularity for the development of components in bio implant applications. However, a comparatively lower hardness, bioactivity and tribo-corrosion resistance property than Ti-6Al-4V has restricted its applications for the development of implants with longer durability[2, 3]. Several surface modification techniques were utilized by the researchers to improve the hardness, wear and corrosion resistance of Ti-13Nb-13Zr alloy. Notable of them include PVD, CVD, ion implantation, thermal spraying and several laser surface engineering processes[4-8].

Among all these surface modification techniques, laser surface treatment offers several advantages in terms of processing finished components with precision, faster processing speed and the development of metastable microstructure. Laser surface treatment may be categorized into laser surface alloying (LSA), cladding, composite surfacing, etc. Laser composite surfacing (LCS) refers to the technique where a composite layer is developed on metallic substrate by in-situ reaction or by external deposition of ceramic particles during laser melting of the surface[9, 10]. In this regard, it may be noted that a defect-free and uniform microstructure is developed only when laser processing is done under a narrow optimum processing region. Hence, it is an important and mandatory step to derive the optimum process parameters of LCS. The optimization tools usually applied for process optimization include Artificial neural networks, ant colony, particle swarm optimization, Taguchi method, etc.[11-14]. Among these techniques, the Taguchi technique is a systematic approach used to design and analysis of experiments to enhance product quality. This approach has emerged as a beneficial tool for achieving high-reliability outcomes in research, as it saves a significant amount of time and material costs[15-17]. Several researchers reported on process parameters optimization of laser surface engineering using Taguchi analysis. Samant *et al.*[18] optimized the microstructural characteristics when laser structuring of alumina using the Taguchi technique. Dubourg *et al.*[19] examined the effects of various cladding parameters

*Corresponding author (Email: jyotsna@metal.iitkgp.ac.in)

on the clad geometry and the WC content using the combination of Taguchi and EM approaches to construct the experimental designs. Lian *et al.*[20] experimented the effect of input parameters on microhardness and wear resistance properties of cladlayer using Taguchi orthogonal approach. With a high degree of statistical precision, the Taguchi method effectively determined the input parameters for LCS process. Consequently, it enabled the development of laser surface alloying process that may get an acceptable dilution ratio[21]. Optimization of process parameters of the composite coatings on WC/INC625 using the laser surfacing process was done by Zhavoronkova *et al.*[22]. Notable studies on laser composite surfacing on titanium and its alloys include development of TiB and TiN dispersed surface on Ti-6Al-4V with 1700 VHN hardness and superior wear and corrosion resistance properties as compared to substrate[23]. Tian *et al.*[24] laser surface alloyed Titanium with TiN-B-Si-Ni mixed powder with a hardness of 1500-1600 VHN. Pang *et al.*[25] laser surface alloyed Ti-6Al-4V with Mo, WC and a mixture of Mo+WC with improved hardness by 87% and sliding wear resistance by 150 times. Wu[26]developed TiC/Ti composite layer on Ti-6Al-4V and reported an improved hardness in addition to wear resistance properties. Though extensive studies were undertaken on LCS of Ti-6Al-4V; however, reported literatures on LCS of Ti-13Nb-13Zr are only a few.

The current study concerns the development of TiC dispersed surface on Ti-13Nb-13Zr alloy by pre-placing graphite slurry and subsequent laser surface melting. Furthermore, a detailed statistical analysis was done correlating the process parameters with the properties like micro-and nanohardness, wear and corrosion resistance for optimization of process parameters by Taguchi analysis.

2 Materials and Methods

In this investigation, Ti-13Nb-13Zr plate (20 mm×20 mm×5 mm) was subjected to sandblasting and coated with graphite (thickness of 250 µm). The pre-coated substrate was subjected to laser melting using a 6 kW continuous wave (CW) fibre optics delivered diode laser with a 3.6 mm beam diameter. Laser processing was conducted at varied power of 1000 -1400 W and scan speed of 10-20 mm/s using an argon shroud. To cover the whole surface with consistent alloyed layer thickness, consecutive melt tracks were overlapped by 25%. The schematic diagram of the laser composite surfacing (LCS) process is shown in Fig. 1. Followed by laser processing, a detailed study of microstructure, phase, and wear resistance properties of laser composite surfaced Ti-13Nb-13Zr were carried out and reported elsewhere[27].

Taguchi technique was applied to design experiments using an L9 orthogonal array. This design was chosen based on two input parameters, each having three levels. The levels of input parameters utilized in the laser composite surfacing (LCS) technique are shown in Table 1.

After LCS, the microstructure of the coupons was characterized by scanning electron microscopy (FEG-SEM, Model: SUPRA 40, Make: Zeiss, Germany). Finally, the mechanical properties like microhardness (Walter UHL, VMHT), nanohardness (Model: Tri-Tec SA Nanoindenter, Make: Anton Paar, Switzerland), wear resistance (against the WC ball) and corrosion resistance (in Hank's solution) were evaluated in details. The characterization of the LCS samples and their properties in terms of microhardness, nanohardness, wear rate and corrosion rate as a function of process parameters are summarized in Table 2.

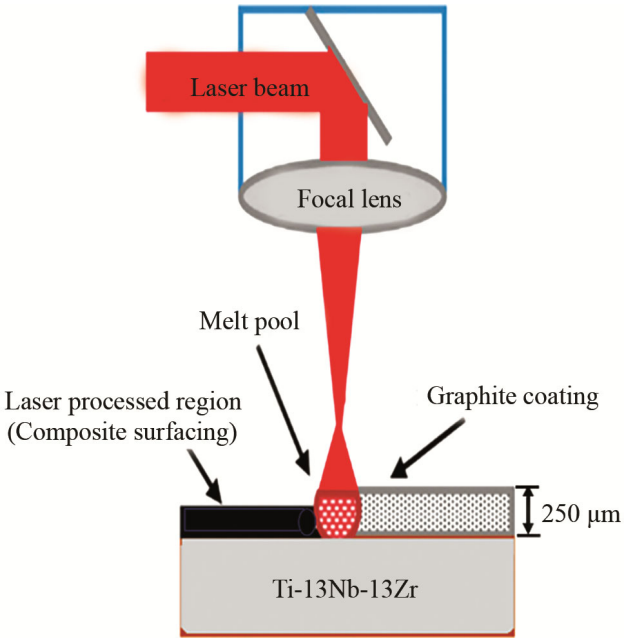

Fig. 1 — Schematic diagram of laser composite surfacing process.

Table 1 — Levels of input parameters used for LCS

Sl No.	Parameter	Level 1	Level 2	Level 3
A	Applied Power (W)	1000	1200	1400
B	Scanning speed (mm/s)	10	15	20

Table 2 — Summary of characteristics and properties of LCS used as output parameters for optimization

Sample Id	Power (W)	Scan speed (mm/s)	Mass fraction of carbides	SDAS (μm)	Micro hardness (VHN)	Nano hardness (GPa)	Wear rate (mm^3/N.m)	Corrosion rate (mm/year)
G1	1000	10	0.408	1.350	413	6.228	0.001278	0.000187
G2	1000	15	0.323	1.167	421	7.061	0.001092	0.000154
G3	1000	20	0.270	0.943	519	9.224	0.000289	0.0001504
G4	1200	10	0.672	1.474	367	5.140	0.000841	0.000341
G5	1200	15	0.341	1.390	365	5.360	0.001150	0.000212
G6	1200	20	0.213	1.283	423	6.845	0.001039	0.000193
G7	1400	10	0.316	1.410	399	5.194	0.000517	0.000390
G8	1400	15	0.314	1.340	360	5.819	0.000797	0.001508
G9	1400	20	0.303	1.306	413	6.801	0.000517	0.000566

Figure 2 (a-f) depicts the contour plots of the process parameters of laser composite surfaced Ti-13Nb-13Zr, showing the effect of laser power and scan speed on (a) mass fraction of carbides, (b) SDAS, (c) microhardness, (d) nanohardness, (e) wear rate and (f) corrosion rate. The contour plot of Fig. 2 (a) shows the variation of carbide mass fraction with power and scan speed. From Fig. 2 (a), it is observed that higher mass fraction of carbide region is observed at intermediate power (1200 W) and low scan speed. In Fig. 2 (b), it may be stated that low power and low scan speed is beneficial in reducing the secondary dendritic arm spacing (SDAS), and the lowest value of the SDAS region is observed at 1000 W applied power and 20 mm/s scan speed. The effect of power and scan speed on microhardness and nanohardness are shown in Fig. 2 (c) and Fig. 2 (d), respectively. Both Fig. 2 (c) and 2 (d) show that higher values of micro and nanohardness region can be observed at 1000 W applied power and 20 mm/s scan speed. However, high laser power (1400 W) is shown to be beneficial in reducing the wear rate of the laser composite surfaced Ti-13Nb-13Zr, as shown in Fig. 2 (e). In Fig. 2 (f), the low corrosion rate region is distributed at low power and throughout the range of scan speed (10-20 mm/s). So, it is challenging to state which processing condition is suitable for improving all output parameters. Hence, optimization of process parameters is essential. In the current study, process parameters are optimized using Taguchi's grey relational analysis, the detailed procedure of which is discussed thoroughly by Kuo *et al*.[28].

2.1 Optimization using Grey Relational Analysis

2.1.1 Calculation of Grey Relational Grade (GRG)

The grey relational analysis (GRA) approach was utilized for process parameters optimization. First of all, the output data was converted into normalized data. The normalization of the output parameters can be calculated using different conditions, such as Larger-the-better and smaller-the-better. Equations 1 and 2 produced normalized data for the Larger-the-better and Smaller-the-better conditions, respectively. The normalized values of output parameters are listed in Table 3.

$$x_i(k) = \frac{y_i(k) - \min y_i(k)}{\max y_i(k) - \min y_i(k)} \quad \ldots(1)$$

$$x_i(k) = \frac{\max y_i(k) - y_i(k)}{\max y_i(k) - \min y_i(k)} \quad \ldots(2)$$

Once a sequence has been normalized, the deviation sequence was calculated following Equation 3 and is summarized in Table 4.

$$\Delta_{oi} = x_0(k) - x_i(k) \quad \ldots(3)$$

The deviation, comparative sequences and reference are denoted by Δ_{oi}, $x_i(k)$ and $x_0(k)$, respectively.

Following that, the grey relational coefficient (GRC) for each data is determined and listed in Table 5.

The GRC may be derived as follows:

$$\varepsilon_i(k) = \frac{\Delta_{min} + \omega\Delta_{max}}{\Delta_{oi}(k) + \omega\Delta_{max}} \quad \ldots(4)$$

Where $\varepsilon_i(k)$ is the grey relation coefficient;

Δ_{min} and Δ_{max} are the smallest and largest value among Δ_{oi}, respectively. ω is the distinguishing coefficient ($0 \leq \omega \leq 1$).

Finally, grey relational grade or GRG (z_i)is obtained by Equation 5. Table 6 represents the GRG of each sample.

$$Z_i = \frac{1}{n}\sum_{k=1}^{n} \varepsilon_i(k) \quad \ldots(5)$$

Table 6 displays the GRG values of all the samples processed under the present study. From the GRG, it may be concluded that the specimenlased with 1000 W applied power and 20 mm/s scan speed offers the

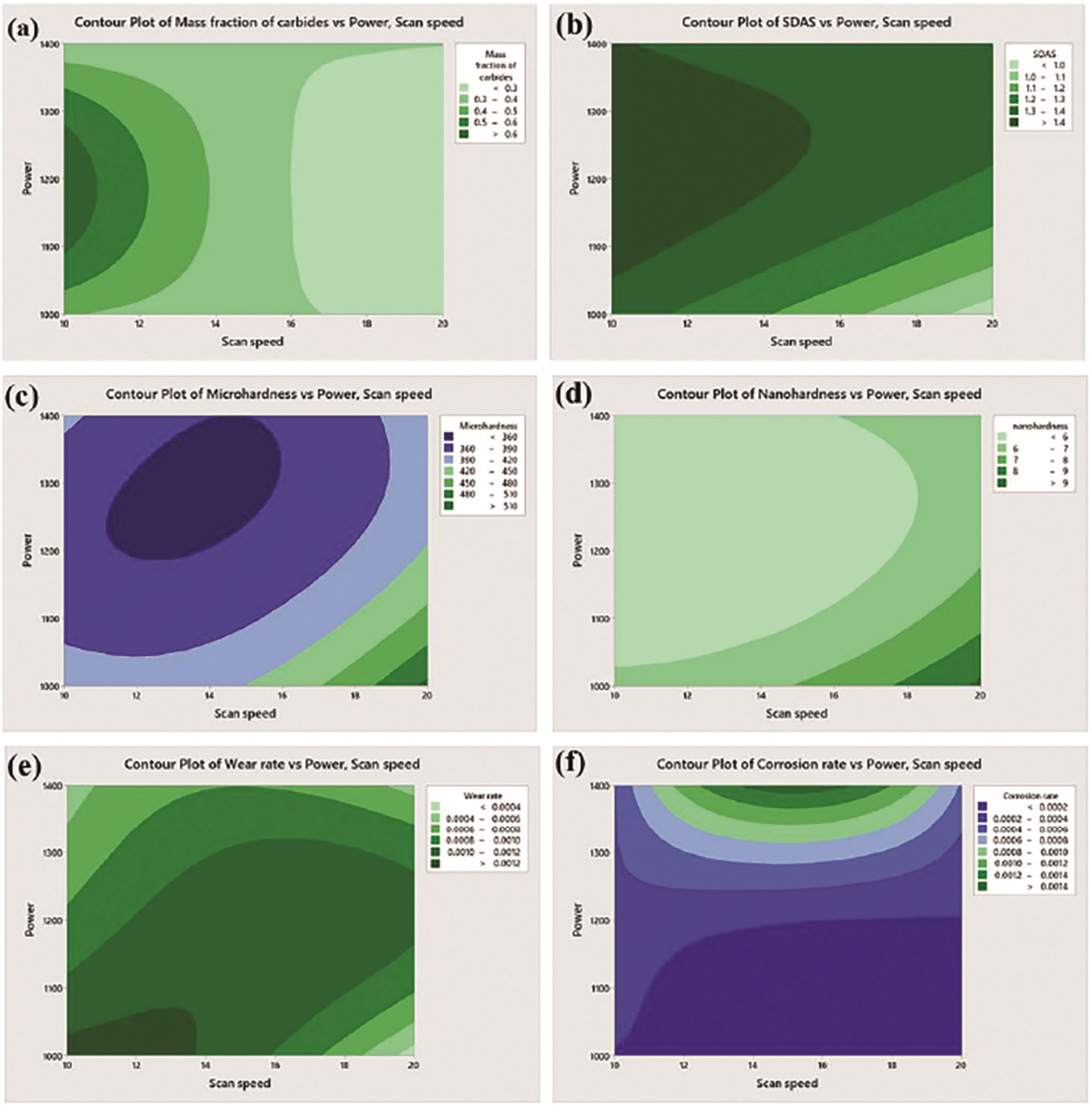

Fig. 2 — Contour plots showing the effect of laser power and scan speed on (a) mass fraction of carbides, (b) SDAS, (c) microhardness, (d) nanohardness, (e) wear, and (f) corrosion rate.

optimum performance in terms of output parameters, as stated above.

2.1.2 Analysis of GRG using S/N Ratio

Taguchi's orthogonal array approach is authentic to optimize the process parameters, which reduces experimental time, and it employs a statistical performance metric, which is termed signal-to-noise ratio (S/N ratio). The S/N ratio for Smaller-the-Better and Higher-the-better were calculated using Equations 6 and 7, respectively.

$$\text{Lower-the-Better: S/N} = -10\log_{10}\frac{1}{n}\sum_{i=1}^{n} y_i^{\,2} \quad \ldots(6)$$

$$\text{Higher-the-better: S/N} = -10\log_{10}\frac{1}{n}\sum_{i=1}^{n}\frac{1}{y_i^{\,2}} \quad \ldots(7)$$

where n and y_i represent the number of experiments and GRG for the i^{th} experiment, respectively.

The mean effect plots of S/N ratio of each output parameter are shown in Fig. 3 (a-f), showing its variation with the power and scan speed. The impact of applied power and scan speed on the mean of the S/N ratio for all output parameters are arranged in the

Table 3 — Normalized values obtained

Sample Id	Mass fraction of carbides	SDAS	Microhardness	Nanohardness	Wear rate	Corrosion rate
G1	0.426	0.233	0.333	0.266	0.000	0.973
G2	0.241	0.578	0.384	0.470	0.188	0.998
G3	0.125	1.000	1.000	1.000	1.000	1.000
G4	1.000	0.000	0.044	0.000	0.442	0.860
G5	0.280	0.158	0.031	0.054	0.129	0.955
G6	0.000	0.359	0.396	0.417	0.242	0.968
G7	0.224	0.120	0.245	0.013	0.769	0.823
G8	0.221	0.252	0.000	0.166	0.486	0.000
G9	0.196	0.316	0.333	0.407	0.769	0.694

Table 4 — Deviance sequence obtained

Sample Id	Mass fraction of carbides	SDAS	Microhardness	Nanohardness	Wear rate	Corrosion rate
G1	0.574	0.767	0.667	0.734	1.000	0.027
G2	0.759	0.422	0.616	0.530	0.812	0.002
G3	0.875	0.000	0.000	0.000	0.000	0.000
G4	0.000	1.000	0.956	1.000	0.558	0.140
G5	0.720	0.842	0.969	0.946	0.871	0.045
G6	1.000	0.641	0.604	0.583	0.758	0.032
G7	0.776	0.880	0.755	0.987	0.231	0.177
G8	0.779	0.748	1.000	0.834	0.514	1.000
G9	0.804	0.684	0.667	0.593	0.231	0.306

Table 5 — GRC of all output parameters

Sample Id	Mass fraction of carbides	SDAS	Microhardness	Nanohardness	Wear rate	Corrosion rate
G1	0.466	0.395	0.429	0.405	0.333	0.949
G2	0.397	0.542	0.448	0.486	0.381	0.995
G3	0.364	1.000	1.000	1.000	1.000	1.000
G4	1.000	0.333	0.343	0.333	0.473	0.781
G5	0.410	0.372	0.340	0.346	0.365	0.917
G6	0.333	0.438	0.453	0.462	0.397	0.941
G7	0.392	0.362	0.398	0.336	0.684	0.739
G8	0.391	0.401	0.333	0.375	0.493	0.333
G9	0.383	0.422	0.429	0.457	0.684	0.620

Table 6 — Grey relational grade (GRG) of all specimen

Sample Id.	G1	G2	G3	G4	G5	G6	G7	G8	G9
GRG	0.496	0.542	0.894	0.544	0.458	0.504	0.485	0.388	0.499
Rank	6	3	1	2	8	4	7	9	5

line graph, where the mean line is indicated by the dashed horizontal. From Fig. 3 (a), it may be stated that the highest mean of S/N ratio of mass fraction of carbides (higher the better) is obtained when laser processed with 1200 W applied power and 10 mm/s of scan speed. Similarly, the mean value of the S/N ratio for secondary dendritic arm spacing (SDAS) (smaller the better) is found during laser processing with 1000 W applied power and 20 mm/s scan speed, as shown in Fig. 3 (b). From Fig. 3 (c) and (d), it may also be depicted that highest mean of S/N ratio for micro- and nanohardness (higher the better) is obtained when laser processed with 1000 W applied power and 20 mm/s scan speed. Fig. 3 (e) shows the mean of the S/N ratio for wear rate where both 1000 W and 1400 W applied power show higher values (smaller the better) of the S/N ratio. But, applied power of 1400 W and scan speed of 20 mm/s is showing maximum value of mean of S/N ratio for wear rate. Also, the maximum values of mean of S/N ratio for corrosion rate (smaller the better) is obtained when laser processed with 1000 W of applied power and 20 mm/s of scan speed.

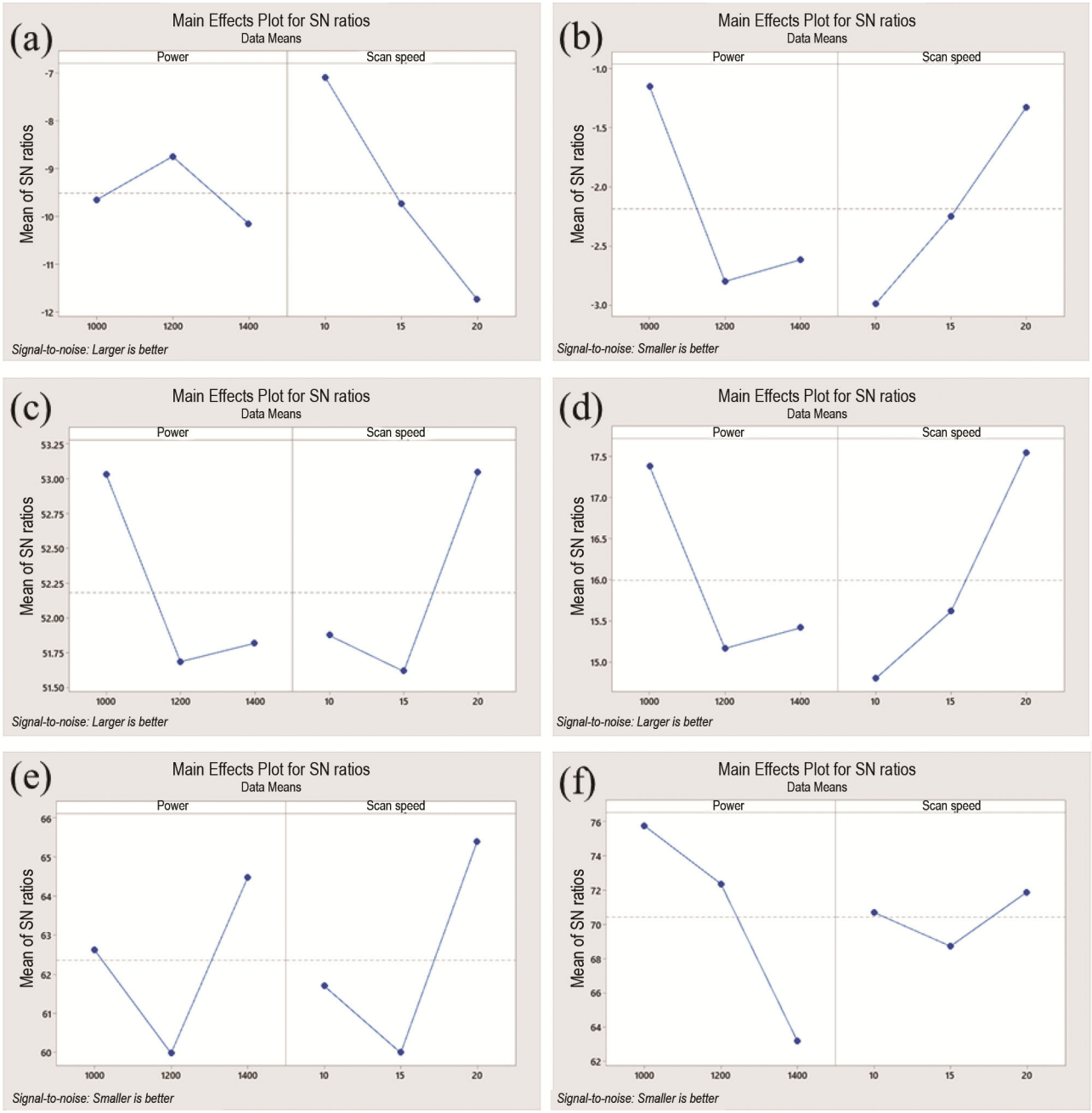

Fig. 3 — Mean effects plot for S/N ratios of (a) mass fraction of carbides, (b) SDAS, (c) microhardness, (d) nanohardness, (e) wear rate, and (f) corrosion rate.

The average GRG values corresponding to input parameters are summarized in Table 6. These were computed by averaging all levels of process parameters for each level group. Because it represents the correlation between the reference and obtained sequences, a higher average GRG suggests a better connection between them. The optimum set of process parameters corresponds to 1000 W applied power and a scan speed of 20 mm/s. In this regard, it may be noted that the highest determining factor contributing to improved performance of the composite surface is applied power followed by scan speed. Figure 4 shows the influence of GRG in terms of the mean of S/N ratios as a function of (a) applied power and (b) scan speed, where the dashed horizontal line in each plot indicates the total mean of GRG. Usually, the larger the GRG, the better the performance characteristics. From Fig. 4 (a, b), it may

be stated that the highest S/N ratio of GRG is obtained when lased at 1000 W applied power and 20 mm/s scan speed. Hence, the results of S/N analysis corroborate the results of Taguchi analysis.

A 3D surface plot of GRG versus power and scan speed is shown in Fig. 5. From Fig. 5, it may be concluded that both power and scan speed influence GRG significantly. While increasing applied power from 1000 W to 1400 W, GRG remains almost constant for10 to 15 mm/s of scan speed. However, GRG has marginal enhancement at 1200 W of applied power and scan speed of 10 mm/s and 20 mm/s, respectively. From Fig. 5, it may further be stated that the highest GRG is obtained during applied power of 1000 W and scan speed of 20 mm/s. Hence, from this statistical 3D plot, it may be concluded that for

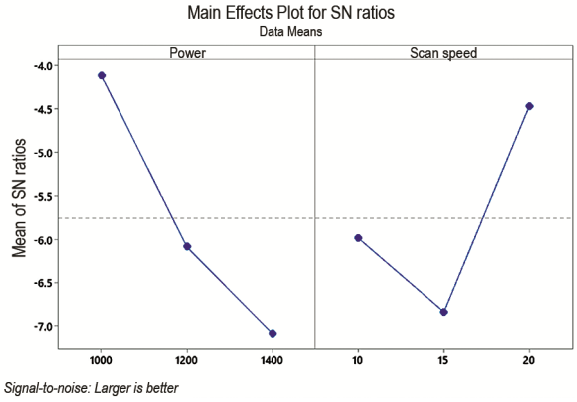

Fig. 4 — Mean effects plot for S/N ratio of GRG.

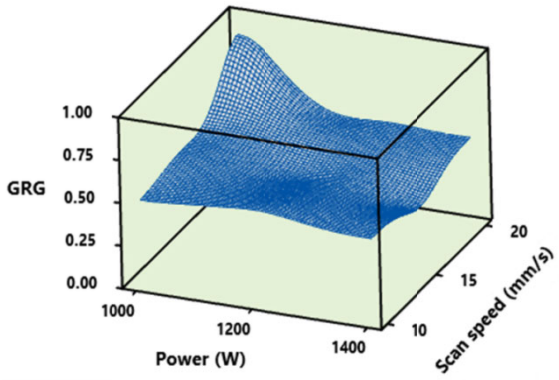

Fig. 5 — 3D surface plot of GRG versus power and scan speed.

LCS of Ti-13Nb-13Zr, the optimum combination of process parameters is 1000 W applied power and 20 mm/s scan speed.

2.1.3 Analysis of Variance (ANOVA) for GRG

The ANOVA (Analysis of Variance) approach was also used to find the effects of applied power and scan speed on GRG values. Table 7 displays the results of the ANOVA of GRG values. From the ANOVA result, it can be stated that the most effective factor affecting the GRG was applied power, which contributed 37.62%. However, Scan speed contributes 30.15% to the GRG.

3 Results and Discussions

3.1 Characteristics and properties of the component processed under optimum process parameters

From the Taguchi analysis and S/N ratio analysis, it was concluded that the sample processed under 1000 W applied power and 20 mm/s scan speed was the optimum process parameter corresponding to maximum hardness, wear and corrosion resistance properties. In this section, a thorough analysis of the microstructure and performance measurement (wear and corrosion resistance) of Ti-13Nb-13Zr followed by LCS processed with 1000 W of applied power and 20 mm/s of scan speed will be discussed in detail.

Figure 6 show the scanning electron micrograph (FEG-SEM) of Ti-13Nb-13Zr laser processed at 1000 W of applied power and 20 mm/s of scan speed. From Fig. 6, it may be explained that the microstructure of the alloyed layer is predominantly dendritic in morphology, with the presence of carbides both in the matrix and also in the dendritic boundaries. The secondary interdendritic arm spacing was found to vary from 0.8 to 1.07 μm with an average value of 0.943 μm, which is the lowest value in comparison to all specimens. Denser and finer carbide precipitation of the optimum sample is the reason behind the improvement in hardness and tribological properties.

Figure 7 summarizes the average microhardness (line plot) and nanohardness (bar graph) plots of as-received and Ti-13Nb-13Zr followed by LCS processed under 1000 W of laser power and 20 mm/s

Table 7 — Analysis of variance of GRG

Source	DF	Seq SS	Adj SS	Adj MS	F	P	%contribution
Power (W)	2	11.602	11.602	5.801	2.33	0.213	37.62
Scan speed (mm/s)	2	9.297	9.297	4.648	1.87	0.267	30.15
Residual Error	4	9.939	9.939	2.485			32.23
Total	8	30.837					

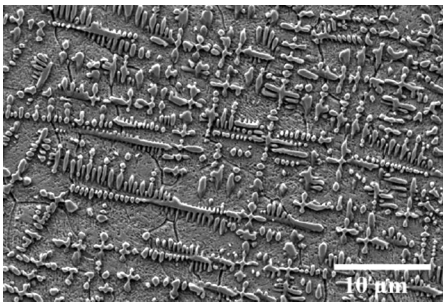

Fig. 6 — Scanning electron microscopic (FEG-SEM) image of laser composite surfaced Ti-13Nb-13Zr lased with 1000 W of applied power and 20 mm/s of scan speed.

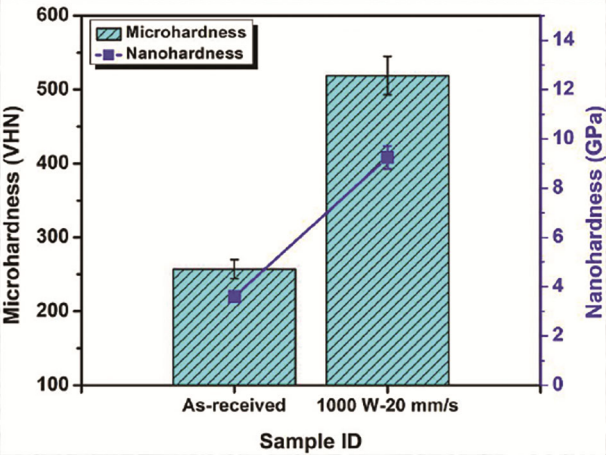

Fig. 7 — Bar chart showing the variation of microhardness and nanohardness of the as-received and Ti-13Nb-13Zr followed by LCS processed at 1000 W applied power and 20 mm/s scan speed.

of scan speed. From Fig. 7, it may be stated that there is a significant improvement in microhardness (519 VHN) and nanohardness (9.224 GPa) of Ti-13Nb-13Zr followed by LCS as compared to the as-received one (257 VHN and 3.5 GPa, respectively). The improvement in both micro- and nanohardness of laser processed Ti-13Nb -13Zr is due to microstructural refinement and precipitate of carbides. The individual contribution of grain refinement and carbide percentage on the microhardness and nanohardness value is under investigation.

Figure 8 summarizes the wear rate (in green) and corrosion rate (in blue) of as-received and Ti-13Nb-13Zr followed by LCS processed under 1000 W applied power and 20 mm/s scan speed. From Fig. 8, it is confirmed that LCS Ti-13Nb-13Zr offers a significant reduction in both the wear and corrosion rate. The improvement in wear resistance is due to grain refinement and carbide precipitations. On the other hand, the corrosion resistance enhancement is attributed to microstructure refinement and homogenization.

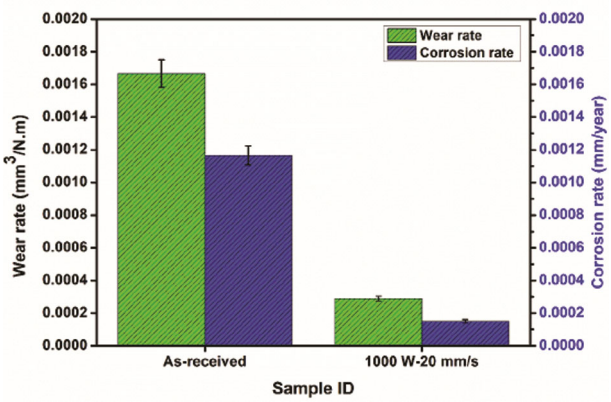

Fig. 8 — Bar chart showing the variation of wear and corrosion rate of as-received and Ti-13Nb-13Zr followed by LCS processed with 1000 W applied power and 20 mm/s scan speed.

3 Conclusions

In this investigation, the experimental design of Ti-13Nb-13Zr followed by LCS, was performed using Taguchi's L9 orthogonal array method. This was followed by a thorough analysis of the characteristics and performance of the composite layer. Finally, parametric optimization was performed using Taguchi's GRA. The S/N ratio was calculated to determine the relevance of process parameters and to validate the results with GRA. The input parameters of the current investigation were applied power and scan speed, and output responses were area fraction of carbides, SDAS, microhardness, nanohardness, wear and corrosion rate. The important findings of the current investigations are summarized below.

- The specimen processed with a power of 1000 W and scan speed of 20 mm/s (G3) shows the best result in terms of refinement of microstructure, maximum hardness and minimum wear and corrosion resistance properties as per GRA.
- S/N ratio of GRG also corroborates the similar result that the sample processed at 1000 W applied power and 20 mm/s scan speed shows a maximum improvement in microhardness, wear and corrosion resistance.
- The microstructure of the sample processed under optimum parameters shows the finer dendritic morphology with the presence of carbides along interdendritic regions and dendritic boundaries. The microhardness, nanohardness, wear and corrosion resistance show a significant improvement in micro- and nanohardness and reduction in wear/corrosion rate as compared to as-received Ti-13Nb-13Zr.

Acknowledgment

Partial financial support from the Science and Engineering Research Board, N. Delhi (POWER Fellowship, SPF/2021/000073, Dt. 11-03-2021), Ministry of Human Resource Development (MHRD), Government of India (under IMPRINT-2, sanction letter IMP/2018/001162, Dt. 02-01-2019), Department of Science and Technology (DST), N. Delhi (DST/TSG/AMT/2015/636/G, Dt. 18-06-2018, DST/TDT/AMT/2017/074 (G), Dt. 12-09-2018), and Alexander von Humboldt Foundation (Friedrich Wilhelm Bessel Award), Bonn, Germany are gratefully acknowledged. Experimental support from ARCI Hyderabad and Central Research Facility, Indian Institute of Technology Kharagpur, is gratefully acknowledged.

References

1 Leyens C & Peters M, (2003).
2 Pitchi CS, Priyadarshini A, Sana G&Narala SKR, Mater Today Proc, 26 (2020) 3297.
3 Chen L-Y, Cui Y-W& Zhang L-C, Metals (Basel), 10 (2020).
4 Krishnan V, Krishnan A, Remya R, Ravikumar KK, Nair SA, Shibli SMA, Varma HK, Sukumaran K& Kumar KJ, ActaBiomater, 7 (2011) 1913.
5 Nakai M, Niinomi M, Tsutsumi H, Saito K & Goto T, Mater Technol, 30 (2015) B8.
6 Vlcak P, Fojt J, Weiss Z, Kopeček J & Perina V, Surf Coatings Technol, 358 (2019) 144.
7 Bansal P, Singh G & Sidhu H, Mater Chem Phys, 257 (2020) 123738.
8 Rossi MC, Amado JM, Tobar MJ, Vicente A, Yañez A & Amigó V, J Mater Res Technol, 14 (2021) 1222.
9 Dutta Majumdar J, Ramesh Chandra B & Manna I, TribolInt, 40 (2007) 146
10 Dutta Majumdar J & Manna I, Sadhana, 28 (2003) 495.
11 Ayeb M, Frija M & Fathallah R, Int J Adv Manuf Technol, 100 (2019) 2455.
12 Hu Y, Liu G, Hao W, Liu Y& Liu Z, J Phys ConfSer, 1187 (2019) 32045.
13 Kalita K, Shivakoti I&Ghadai RK, Mater Manuf Process, 32 (2017) 1101.
14 Zhang Z & Kovacevic R, JOM, 68 (2016) 1762.
15 Tong L, Su C & Wang C,Int J Qual Reliab Manag, 14 (1997) 367.
16 Bera T&Das S, Indian Weld J, 55 (2022) 60.
17 Ogbonna O, Akinlabi S, Madushele N, Fatoba O & Akinlabi E, Int J Adv Manuf Technol, 126 (2023) 1.
18 Samant AN, Paital SR&Dahotre NB, J Mater Process Technol, 203 (2008) 498.
19 Dubourg L& St-Georges L, J Therm Spray Technol, 15 (2006) 790.
20 Lian G, Zhao C, Zhang Y, Feng M& Jiang J, ApplSci, 10 (2020) 3167.
21 Ng KW, Man HC, Lawrence J & Yue TM, Proc Inst Mech Eng Part B J Eng Manuf, 223 (2009) 969.
22 Zhavoronkova E, Alekseev A, Bazaleeva K & Pakhomova S, E3S Web Conf, 376 (2023).
23 SenthilSelvan J, Subramanian K, Nath AK, Kumar H, Ramachandra C & Ravindranathan SP, Mater SciEng A, 260 (1999) 178.
24 Tian YS, Chen CZ, Wang DY, Huo QH& Lei TQ, Appl Surf Sci, 250 (2005) 223.
25 Pang W, Man HC & Yue TM, Mater Sci Eng A, 390 (2005) 144.
26 Wu WL, Mater Sci Technol, 26 (2010) 367.
27 Bera T, Manna I, & Dutta Majumdar J, *J Mater Process Technol, 328* (2024) 118394.
28 Kuo Y, Yang T& Huang G-W, Comput Ind Eng, 55 (2008) 80.